Thermal and population lensing of Yb:YLF at cryogenic temperature

MUHARREM KILINC,[1,2,*] UMIT DEMIRBAS,[1,2] JUAN B. GONZALEZ-DIAZ,[1] JELTO THESINGA,[1] MARTIN KELLERT,[1] GUIDO PALMER,[1] FRANZ X. KÄRTNER,[1,3,4] AND MIKHAIL PERGAMENT,[1]

[1]*Center for Free-Electron Laser Science CFEL, Deutsches Elektronen-Synchrotron DESY, Notkestr. 85, 22607 Hamburg, Germany*
[2]*Department of Electrical and Electronics Engineering, Antalya Bilim University, 07190 Dosemealti, Antalya, Turkey*
[3]*Physics Department, University of Hamburg, Luruper Chaussee 149, 22761 Hamburg, Germany*
[4]*The Hamburg Centre for Ultrafast Imaging, Luruper Chaussee 149, 22761 Hamburg, Germany*
**muharrem.kilinc@desy.de*

Abstract: We present what is, to our knowledge, the first detailed study of thermal and population lensing in cryogenically cooled Yb:YLF. Using a rod-shaped a-cut Yb:YLF crystal, the thermal lens strength is measured as a function of absorbed pump power for both E//a and E//c polarizations for pump power levels up to 600 W. Our experiments revealed that the thermal lensing behavior in Yb:YLF is quite asymmetric. For the E//a polarization, the thermal lens is rather strong and always converging for both horizonal and vertical axes. For the E//c configuration, thermal lensing is rather weak, and its sign could be different in different axis, and furthermore, the sign of thermal lensing is observed to be dependent on the absorbed pump power level. Simulations and detailed experimental measurements show that the observed peculiar behavior is a result of competition between the photo-elastic effect and thermo-optic effect: as their relative strength varies at different pump power levels. We have also measured the contribution of surface bulging into thermal lensing and found it to be relatively small in our crystals with un-doped end caps. Lastly, the population lensing is measured in Yb:YLF for the first time, and it is found to be quite weak as well, and the polarizability difference parameter of Yb:YLF is determined as (3±1.5) x 10^{-34} m^3.

1. Introduction

High-power diode end-pumped cryogenically cooled solid-state lasers stand out with their improved laser efficiencies, good output beam qualities, and extreme average and peak power levels [1–9]. Compared to room-temperature systems, cryogenic operation increases laser emission cross section, boosts up thermal conductivity, lowers thermal expansion coefficient, reduces thermo-optic effect, and minimizes wavefront distortions, and enables power scaling in simpler laser architectures [10,11]. Using the leverage of cryogenic operation, average powers from Yb:YLF systems are scaled up to 600 W in continuous-wave lasing operation and to 350 W level in regenerative amplification even by employing simple rod-shaped gain elements [6–9,12–15]. Despite the demonstrated advantages of cryogenic cooling [1,8,15–17], thermally-induced lensing is still the main limiting factor for further power scaling, and hence detailed understanding of it is crucial.

There are four main lensing mechanisms in high power laser systems (ignoring Kerr lensing, which is ideally eliminated via chirped pulse amplification (CPA) [18]). Three of these lensing mechanisms are thermally driven, and one is due to electronic interactions:

(i) Thermo-optic effect (dn/dT): Thermo-optic effect is based on temperature dependence of refractive index of the laser gain media [11,19,20]. Pumping of the laser gain media

results in a position dependent temperature profile: a higher temperature increase occurs in the pumped regions. Therefore, a larger change in the refractive index appears in the center of the pumped region compared to the edges. Hence, the laser light passing through the gain element observes a position dependent optical path length. If the dn/dT coefficient is positive, one observes a positive (convex) lens since the optical path length in the center of the optical axis would be longer. If the dn/dT coefficient is negative, one acquires a negative (concave) lensing.

(ii) Bulging of the end faces: When the materials are heated, they tend to expand, and the amount of expansion depends on temperature rise. The temperature inside the laser gain media is not homogeneously distributed even for a pump that has a flat-top intensity profile. Since the center of the pump region gets hotter compared to the outer region, it expands more. Therefore the surface/s of the crystal act like a positive lens, which is called the bulging lens effect [21–23].

(iii) Photo-elastic effect: Thermally induced mechanical stress occurs because of the non-uniform temperature distribution (temperature gradients) in laser gain media. That stress causes thermal birefringence due to the photo-elastic effect and influences the refractive index of the material. Hence it causes lensing which is called stress-induced thermal lensing, or photo-elastic effect lensing [24,25]. To calculate it, the photo-elastic coefficients for the corresponding material must be known.

(iv) Population lensing: The last contribution to the total lensing effect is the population lensing, which is also known as electronic lensing [26–28]. The refractive index response of the materials differs depending on whether the ions are in the excited state or in the ground state due to the difference in polarizability of the active ions [27,29,30]. Since it is directly proportional to the number of excited laser active ions in the laser upper state, it creates a curvature depending on the pump beam profile (Gaussian pump, flat top pump, etc.), and that curvature induces the population lensing effect.

So far, thermal lensing studies have been performed for several Yb-doped hosts including YAG [30–33], YAB [34], YCOB [32,35], KGW [32,36], $KLu(WO_4)_2$ [37,38], $KY(WO_4)_2$ [39], GdCOB [32], and YSO [32]. Among these hosts, studies have shown that YLF host is one of the most suitable candidates for power scaling [16,17], mainly due to its negative dn/dT coefficient, which results in a relatively weak total thermal lensing [17,24,39]. There are some earlier studies of YLF hosts thermal lens behavior at room-temperature in several laser active gain media such as Pr:YLF [40], Nd:YLF [25,41–44], Tm:YLF [45,46] and Tm:Ho:YLF [47], but to our knowledge, population and bulging lensing in YLF is not measured yet, and literature still lacks a detailed investigation of thermal lens behavior of Yb:YLF medium at cryogenic temperatures.

In this work, we have investigated the polarization-dependent total thermal lens strength of a 1% Yb-doped YLF in rod geometry at cryogenic temperatures while employing conditions similar to what is used in our previous lasing/and amplification studies [8,9] (2.1 mm diameter pump beam in a 2 cm long crystal). For E//a polarized light, the total thermal lens is measured as 2.6 m and 3.8 m at 500 W of absorbed pump power, for horizontal and vertical axis, respectively. For E//c polarization, the total thermal lens is measured as -10.4 m and 10 m for horizontal and vertical axis, at the same absorbed pump power level. To understand the observed asymmetric and peculiar behavior, we have then tried to identify the strength of different contributions to the total thermal lensing. We have started with measuring the population lensing strength of Yb:YLF, and it is found to be quite weak (550 m at 500 W of absorbed pump power). The corresponding polarizability difference parameter of Yb:YLF is determined as 3×10^{-34} m^3, that is around 30-fold smaller than the value for Yb:YAG (88×10^{-34} m^3). The thermal lensing due to surface bulging is also measured to be rather weak

(125 m at 500 W of absorbed pump power for the front surface of the crystal), due to the undoped caps used on both ends of the crystal. Hence, we have determined that the total thermal lensing of Yb:YLF is mainly due to the thermo-optic and photo-elastic effects. The thermo-optic coefficient of YLF is negative for both E//a and E//c polarizations, but it is smaller for E//a axis [11]. Via detailed numerical analysis, we have shown that for E//a polarized light, the thermal lens due to photo-elastic effect (1.4 m) is larger compared to the thermo-optic effect (-2.9 m), and this results in a positive overall thermal lens (2.6 m, for horizontal axis, at an absorbed pump power of 500 W). On the other hand, for E//c polarized light, the thermal lens due to thermo-optic effect (-1 m) could be as strong as photo-elastic effect (1.1 m), and one obtains a relatively weak overall total thermal (-10.4 m for horizontal axis, at an absorbed pump power of 500 W). For E//c polarized light, since the strengths of photo-elastic effect and thermo-optic effect is similar, the sign of the overall thermal lens oscillates with absorbed pump power level (or crystal temperature): it is weak and positive at low pump power levels and weak and negative at absorbed pump powers above 300 W. We believe that the findings presented in this study will be very useful in further power scaling of cryogenic Yb:YLF based lasers and amplifiers.

2. Experimental methodology

A simplified schematic of the setup used for thermal and population lensing measurements is shown in Fig. 1. The 1% Yb-doped YLF crystal is 20 mm long, 20 mm wide, and 15 mm thick. The crystal has 3 mm thick undoped end-cap regions on both ends to minimize surface bulging (increasing the total length to 26 mm). An a-cut Yb:YLF sample is used to access the thermal lensing behavior in both E//a and E//c polarizations. A 960 nm fiber-coupled diode system with up to 3 kW of continuous-wave (CW) output power is utilized as the pump source. The thermal lensing of the Yb:YLF crystal is measured using two different methods. In both methods, a linearly polarized 1064 nm probe beam is coupled into the system through the dichroic mirrors (DM1-DM2). The probe beam co-propagates with the pump beam within the crystal, and both have a beam waist of around 2.1 mm (the pump beam is focused at the center of the crystal). This pump beam parameters are identical to what was used in our previous lasing/and amplification studies [8,9], and enables us to put a spotlight on thermal lens limitations for further power scaling of rod-based cryogenic Yb:YLF system.

As the first method for thermal lens measurement, the probe beam is imaged to the HASO4 FIRST Wavefront Sensor (WFS), manufactured by Imagine Optic, utilizing 4-f geometry [26]. The wavefront profile captured by the sensor is then analyzed at varying absorbed pump power levels to deduce the thermal lens information. The 4-f imaging system is carefully adjusted to image the wavefront of the probe beam just after the crystal, so the total lensing of the crystal can be measured. Furthermore, the 4-f system provides a constant beam size on the WFS, and hence with adequate magnification the full active area of the WFS could be utilized for higher accuracy measurements (aperture dimension= 3.6 x 4.6 mm^2, spatial resolution$\cong$ 110 μm). The wavefront sensor detects the changes in the wavefront at different absorbed pump power levels, and resultant wavefronts are spherically fitted to calculate the thermal lens strength. As a second approach, the wave-front sensor and the 4-f imaging lenses (f6-f7) are removed, and a high resolution (2048 × 2048 pixels) beam profiler camera (DAT-WinCamD-LCM) is used to record the variation of transmitted probe beam size with absorbed pump power level. Then, the strength of the thermal lens induced inside the laser crystal is calculated using ABCD matrix beam propagation formalism for Gaussian beams.

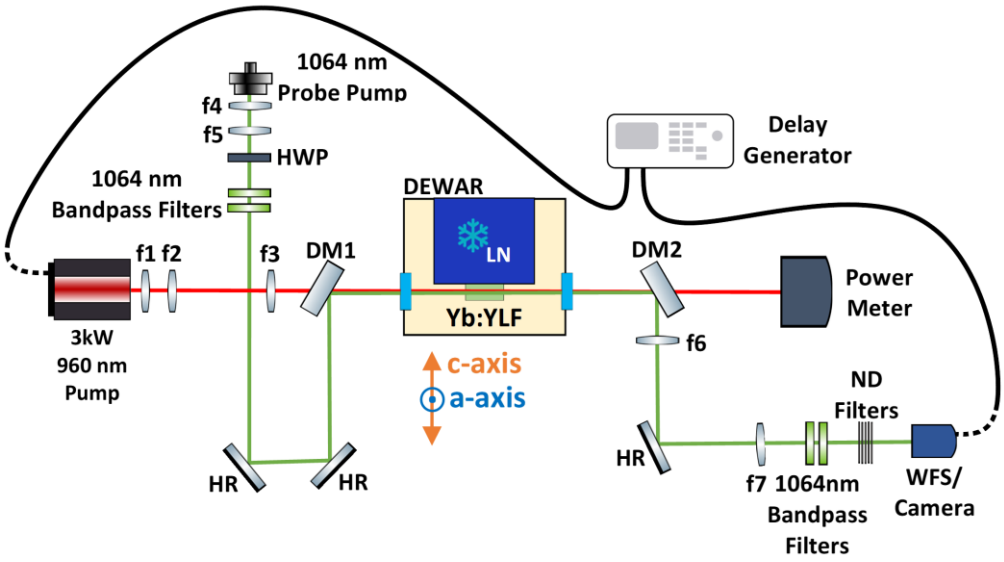

Fig. 1. A simplified schematic of the setup used in population and thermal lensing measurements. f1-f3: 960 nm pump beam shaping optics, f4-f5: Collimating lenses for the probe beam, f6-f7: 4f imaging optics used to image the probe beam into the wavefront sensor. ND: Neutral density filters, WFS: Wavefront sensor, DM: Dichroic mirror, HR: High reflector, HWP: Half-wave plate.

For population lensing measurement, the pump beam is modulated using a delay generator to provide 950 ms long pulses at a 1 Hz repetition rate. This enabled pumping close to CW pumping conditions as the duty cycle is at 95% level. The remaining open window (50 ms) is used to investigate the decay characteristics of the thermally induced wavefront aberrations to extract information on population lensing. Basically, the contribution of the population lens on the wavefront should reduce as the excited ions on the upper-level decay back to the ground state. For Yb:YLF, the fluorescence lifetime of the crystal is around 2 ms at cryogenic temperatures [48], and in the same time scale the population lensing effect should also decay. The thermal lensing on the other hand will decay in a much longer time scale, as the temperature of the crystals decreases much more slowly in 10s of milliseconds, as the crystal at hand is rather bulky and it has a large thermal time constant. Hence, the measured time decay of optical path difference could be modeled using:

$$\mathrm{OPD}(t) = A_{th} * e^{-\frac{t}{\tau_{th}}} + A_p * e^{-\frac{t}{\tau_p}} \quad (1)$$

where t is time, A_{th} and A_p are the strength of thermal and populating lensing contribution to optical path difference, and τ_{th} and τ_p are their relevant decay times. Once the optical path difference caused by the population lensing is determined ($\mathrm{OPD}_{popul}(x,y)$), the polarizability difference ($\Delta\alpha$) parameter could be estimated using:

$$\mathrm{OPD}_{popul}(x,y) = \frac{2\pi}{n_0}\left(\frac{n_0^2+2}{3}\right)^2 \Delta\alpha \int_0^L N_2(x,y,z)\,dz\,. \quad (2)$$

In Eq. (2), $N_2(x,y,z)$ is the inversion density as a function of position inside the gain element, n_0 is the intrinsic refractive index and L is the length of the gain material.

The thermal lens contribution that comes from the surface bulging of the end faces is also measured by employing a slightly modified setup as shown in Fig. 2. For this case, the probe beam is used in reflection geometry to measure the surface profile of the crystal under thermal load. Since the Yb:YLF crystals are anti-reflection coated around 1 µm, a 543 nm probe beam is used for this measurement. The rest of the setup has the same approach that we have in the setup of total thermal lensing measurement.

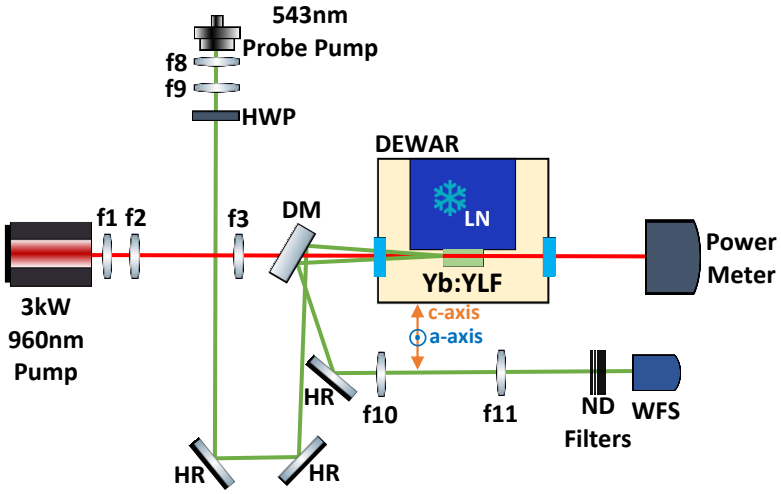

Fig. 2. A simplified schematic of the setup used in the surface bulging-induced thermal lensing measurement.

Finally, in our numerical analysis, the thermal lensing effect that is driven by the temperature-dependent refractive index is calculated using:

$$\mathrm{OPL}_{\mathrm{thermoOptic}}(\mathrm{x},\mathrm{y}) = \int_0^{\mathrm{L}} \left(\int \frac{dn(\mathrm{T}(\mathrm{x},\mathrm{y},\mathrm{z}))}{dT}.dT\right)\mathrm{dz} \qquad (3)$$

where $\mathrm{OPD}_{\mathrm{thermoOptic}}(\mathrm{x},\mathrm{y})$ is gives position dependence of optical path distortions acquired due to the thermo-optic effect, $\frac{dn}{dT}$ is the thermo-optic coefficient as a function of temperature [11], $\mathrm{T}(\mathrm{x},\mathrm{y},\mathrm{z})$ is the position-dependent temperature inside the crystal, and L is the length of the material.

3. Experimental Results and Discussion

3.1 Total thermal-lens measurements

Fig. 3 summarizes the overall thermal lens measurements performed with Yb:YLF using the wavefront sensor method. The wavefront sensor measures the optical path difference acquired by the probe beam in 2-dimensions. As an example, Fig. 3 (a) and (b) show the measured wavefront for E//c and E//a polarized light at an absorbed pump power of 600 W. The measured wavefronts are clearly not flat due to the thermal lens observed by the probe beam while passing through the Yb:YLF crystal. As we can already see from Fig. 3 (a-b): (i) for E//a polarization, the phase acquired is mostly symmetric, has a shape of elliptic paraboloid, and shows positive thermal lensing behavior for both axes, (ii) whereas for E//c polarization the phase profile has a hyperbolic paraboloid shape, and the beam is converging in vertical axis and diverging in horizontal axis. To investigate the variation of the thermal lens with pump power, wavefront data such as that is shown in Figs. 3 (a-b) is taken for absorbed pump powers in the 100-600 W

range. Figs. 3 (c-f) show 1-dimensional cut-throughs extracted from the measured wavefront data along both vertical and horizontal axes at different absorbed pump power levels. The measurements indicate that the wavefront distortion is much weaker for E//c polarized light in both horizontal and vertical directions as compared to the E//a polarization (the magnitude of the OPD is around 3 times smaller for E//c polarization). In the horizontal direction of the E//c polarization, an interesting behavior is observed: the wavefront distortions are positive up to 300 W, and above this power level the distortion changes sign to negative and increases progressively with increasing power levels. In contrast, the wavefront distortions in the E//c orientation in the vertical direction are always positive and exhibit a cumulative increase with power.

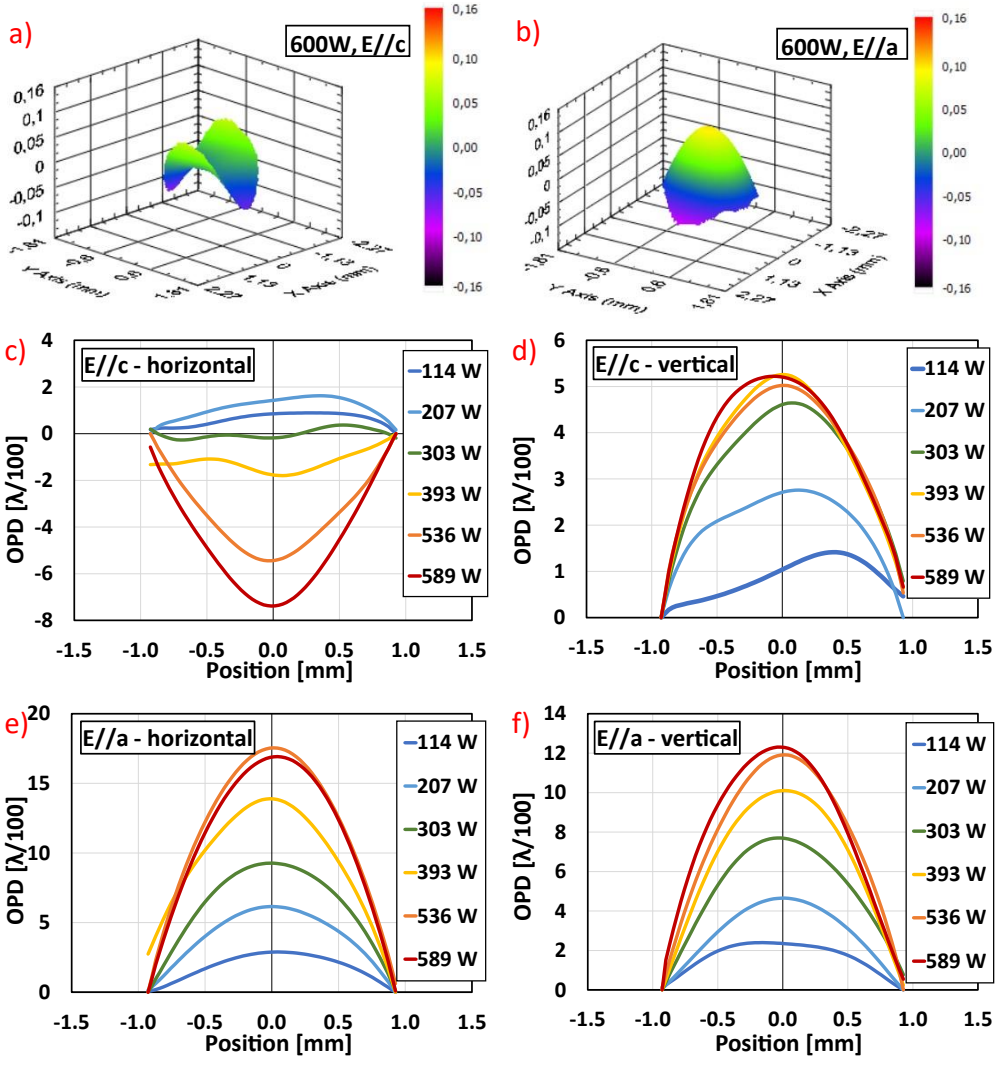

Fig. 3. (a-b) Measured wavefront distortions of Yb:YLF crystals in 2-D for an absorbed pump power of 600 W (screenshots from the interface of WFS). (c-e) Measured 1-D variation of the optical wavefront distortions as a function of absorbed pump power. The measurements are taken for incident light polarized in E//c (a-c-d) and E//a (b-e-f) axes. Moreover, due to the asymmetry of the thermal lens, measurements have been performed both for the horizontal and vertical directions.

As indicated earlier, as a second approach, we have also measured the variation of transmitted probe beam shape with absorbed pump power to investigate thermal lensing. Fig. 4 shows the measured probe beam profiles for E//c and E//a polarizations at pump powers up to 600 W. The measurement has been repeated twice, at crystal-to-camera separations of 1 m and 1.45 m to confirm the validity of the measurement. Fig. 4 also includes information on the measured beam diameters for each data point. Looking at the variation of beam size at different pump power levels, a clear positive and rather symmetric thermal lens behavior is visible for E//a polarized light (Fig. 4 (b-d)). On the other side, for E//c polarized probe light, we see a converging beam in vertical axis and diverging beam in horizontal axis (Fig. 4 (a-c)). So, clearly both approaches for thermal lens measurement indicate similar trends in thermal lens behavior, confirming each other.

a) **Camera @ 1 m**

E//c

Power (W)	0	114	159	207	256	303	348	393	434	471	505	537	566	589
Intensity Profile	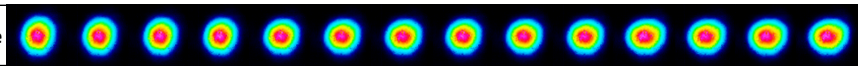													
Beam Diameter (hor) (mm)	2.17	2.11	2.15	2.13	2.14	2.16	2.18	2.21	2.27	2.28	2.37	2.42	2.45	2.51
Beam Diameter (ver) (mm)	2.42	2.34	2.32	2.29	2.25	2.23	2.22	2.20	2.18	2.18	2.20	2.19	2.14	2.14

b) **Camera @ 1 m**

E//a

Power (W)	0	114	159	207	256	303	348	393	434	471	505	537	566	589
Intensity Profile	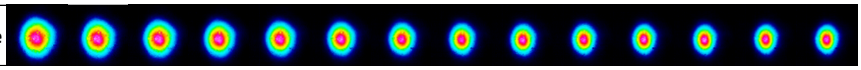													
Beam Diameter (hor) (mm)	2.21	2.04	1.99	1.90	1.81	1.72	1.67	1.56	1.55	1.44	1.42	1.42	1.37	1.39
Beam Diameter (ver) (mm)	2.53	2.35	2.29	2.15	2.08	2.01	1.95	1.94	1.87	1.86	1.82	1.83	1.81	1.82

c) **Camera @ 1.45 m**

E//c

Power (W)	0	115	160	207	256	303	348	392	434	471	505	537	566	589
Intensity Profile	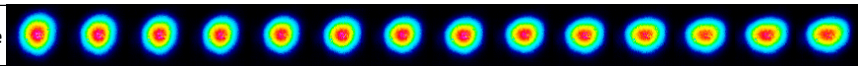													
Beam Diameter (hor) (mm)	2.20	2.20	2.18	2.16	2.18	2.21	2.28	2.35	2.40	2.44	2.53	2.61	2.67	2.71
Beam Diameter (ver) (mm)	2.50	2.39	2.32	2.26	2.23	2.25	2.20	2.21	2.23	2.17	2.18	2.17	2.22	2.18

d) **Camera @ 1.45 m**

E//a

Power (W)	0	114	159	207	256	303	348	393	434	471	505	537	566	589
Intensity Profile	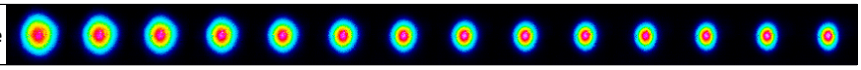													
Beam Diameter (hor) (mm)	2.29	2.08	2.02	1.94	1.82	1.70	1.59	1.53	1.45	1.34	1.31	1.29	1.25	1.24
Beam Diameter (ver) (mm)	2.63	2.43	2.35	2.26	2.11	2.03	1.96	1.87	1.82	1.75	1.70	1.69	1.66	1.65

Fig. 4. Transmitted beam profile of the probe beam at different absorbed pump power levels. Horizontal and vertical beam diameters and intensity profiles of the probe beam are measured for E//c polarization at (a) 1 m, (c) 1.45 m, and for E//a polarization at (b) 1 m, (d) 1.45 m.

To look at the data more qualitatively, Fig. 5 shows the measured variation of overall thermal lensing in cryogenic Yb:YLF rod as a function of absorbed pump power level using both the

wavefront sensor method and beam profile method. As we can see, the results obtained from both the wavefront sensor and camera exhibit strong agreement with each other, for both input polarizations and axes, which confirms the validity of the results. As also discussed above briefly, we see that the magnitude of the thermal lensing effect is consistently larger for the E//a polarized light as compared to the E//c polarized light. In addition, for E//a polarization, the measured thermal lens is always positive and exhibits a rather symmetrical pattern, with comparable strengths observed in both horizontal and vertical axis. For the E//c polarized light, the thermal lens is weaker, and its behavior differs based on axes: (i) in the vertical axis, the thermal lens is consistently positive, and the rate at which it increases exhibits a tendency to saturate at absorbed pump power above 300W, and (ii) in horizontal axis, the thermal lens is initially small and positive for absorbed pump power up to 300W, and beyond this point, the thermal lens changes sign, becoming negative and increasingly stronger. The observed behavior can be attributed to the temperature dependence of the thermo-opto-mechanical coefficients of the YLF host, as discussed in prior literature [11,25]. In order to gain a more comprehensive understanding of the polarization and axis-dependent lensing effect in Yb:YLF, we have performed further measurements to understand the role of different lensing mechanisms in the observed behavior.

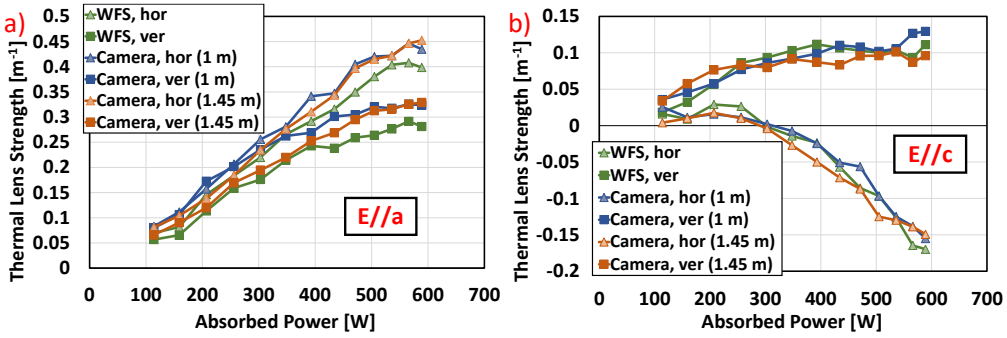

Fig. 5. Measured thermal lens strength as a function of absorbed pump power in cryogenic Yb:YLF. The data is shown for (a) E//c and (b) E//a polarizations, both in horizontal and vertical directions.

To start with, we have first measured the contribution of population lensing (also known as electronic lensing or pump induced waveform aberrations) into the overall measured lens strength, as reports indicate that this could be rather effective in well-known systems like Yb:YAG, Yb:KGW, and Yb:YVO_4 [49]. To our knowledge, population lensing was not measured in any YLF host before. Hence, to validate our experimental methodology, we have also performed measurements with a cryogenically cooled Yb:YAG sample with identical properties (2 cm length, 1% Yb-doping), where one can find some initial population lensing data. Figs. 6 (a-b) show the measured time-dependent variation of the wavefront distortions for Yb:YLF and Yb:YAG at an absorbed power level of 500 W and 220 W, respectively. From the measured data, we have determined the decay dynamics of the optical path difference during the 50 ms off-time for both gain materials, as shown in Figs. 6 (c-d). Note that, we looked at the decay of optical distortions around the center of the crystal, where the change is maximum. As previously mentioned, the acquired optical path difference might be due to population and thermal effects and they decay with their characteristic time scales. To distinguish between the two, we fit the experimental data using a double exponential decay model (Eq. 1) and extract the respective contributions of the thermal and population lensing effects.

For Yb:YLF, the thermal part of the wavefront distortions decay in roughly 90 ms while population lensing decays in around 2 ms (fluorescence lifetime of 1% Yb doped YLF at cryogenic temperatures [48,50]). By using the measured population lensing strength and Eq. 2, the polarizability difference of Yb:YLF is then calculated as $(3 \pm 1.5) \times 10^{-34}$ m^3. The same

analysis was repeated for Yb:YAG to confirm our measurement technic, and the resulting value for the polarizability difference is (88 ± 40) x 10^{-34} m^3. The value we have estimated for YAG is close in magnitude to the reported value for the polarizability difference by Antipov et al., which is (190 ± 80) x 10^{-34} m^3 [51]. We believe that the difference between the reported values might be due to the temperature dependency of polarizability difference parameter as the reported study in [50] was conducted at room temperature while our study was performed at cryogenic temperatures. In short, we see that the population lensing effect is much weaker in Yb:YLF compared to Yb:YAG. Due to the weaker polarizability difference, the resulting optical path difference from Yb:YLF (647 m lensing) is much weaker than that from Yb:YAG (60 m lensing) when both are subjected to an absorbed power of 500 W, as shown in Fig. 6(e). This measurement shows that, one can safely ignore the contribution of population lensing in Yb:YLF, as its strength is almost two orders of magnitude smaller compared to the measured overall lens strength.

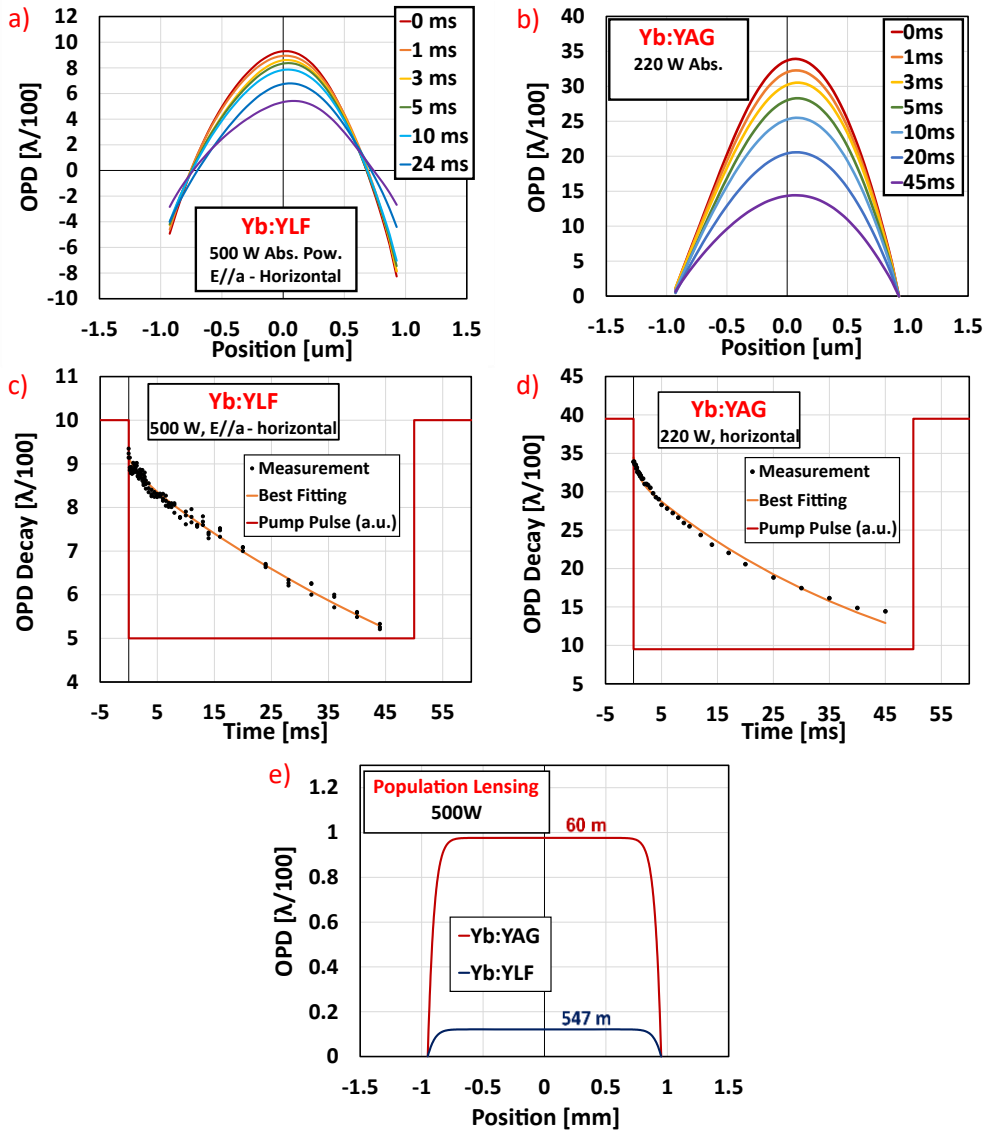

Fig. 6. Measured time-dependent variation of the optical wavefront distortions in (a) Yb:YLF and (b) Yb:YAG. The decay dynamics of the maximum differential optical path difference acquired is shown in (c-d). The measurements are taken for (a-c) Yb:YLF and (b-d) Yb:YAG for an absorbed power of 500 W and 220 W, respectively. The time-dependent data can be used to differentiate the contributions of electronic and population lensing. (e) Estimated OPDs from population lensing (electronic effect) for Yb:YLF and Yb:YAG.

The contribution of bulging to total thermal lensing is also measured (Fig. 7(a)). Since there are two end faces of the crystal, measurements are taken from both the front and back surfaces. Note that in our crystal, we have undoped end caps in both front and back surface of the Yb:YLF crystal to minimize bulging. Hence, compared to crystals without undoped cap regions, the expected bulging is also quite weak. In our measurements, we have found that the contribution of bulging from the front surface to the total lensing is rather weak (125 m). Also, due to one side pumping, the bulging effect is much weaker in the back surface compared to the front surface of the crystal, since most of the power is absorbed in the beginning of the crystal due to the high absorption cross-section of Yb:YLF at cryogenic temperatures (even considering the pump saturation effect) [10]. As a result, the measured contribution of bulging from the back surface is negligible and falls within the noise level (< 1 nm). Fig. 7(b) shows the simulated bulging of the end faces, which is found to be consistent with the measurements. The simulation predicts 68 m lensing from the front surface, while the back surface shows almost no wavefront distortion or lensing effect, which is consistent with our experimental results. As a result, we see that, similar to population lensing, the thermal lensing due to surface bulging is also quite weak for Yb:YLF in our pumping geometry.

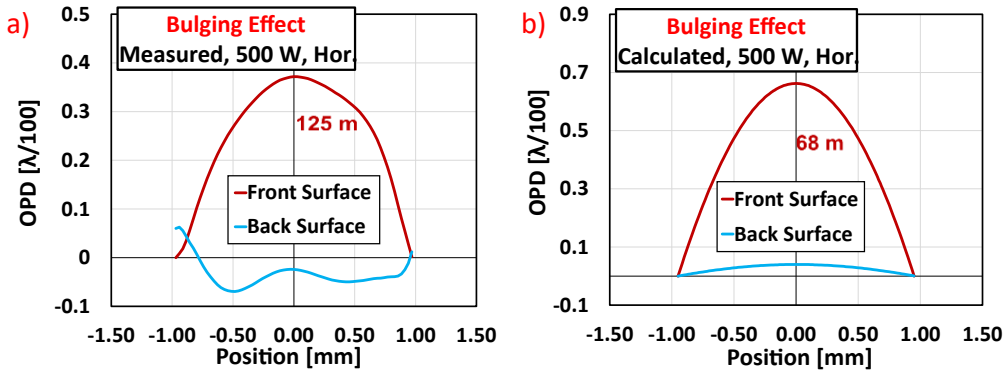

Fig. 7. (a) Measured and (b) calculated OPDs of the bulging effect of front and back surfaces of Yb:YLF at an absorbed power of 500W.

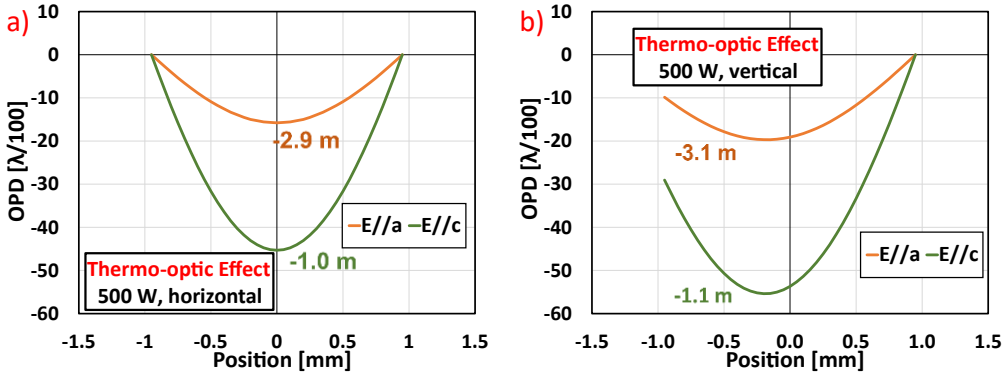

Fig. 8. Calculated polarization dependent OPDs of thermo-optic effect for (a) horizontal and (b) vertical directions at an absorbed power of 500W.

The remaining contributions to the overall thermal lensing are then lensing due to thermo-optic and photo-elastic effects. The temperature-dependent thermo-optic coefficient (dn/dT) was previously reported by Aggarwal et al. [11]. By simulating the temperature distribution inside the crystal, lensing due to the thermo-optic effect can then be estimated using Eq 3. The calculated lensing effects (optical path differences acquired) resulting from the thermo-optic contribution are shown in Fig. 8 for both horizontal and vertical directions of light with polarization E//a and E//c. It is noteworthy that the lensing effects are negative in all cases due to the negative thermo-optic coefficients of the YLF host. Moreover, the optical path distortion is more pronounced in the vertical and horizontal directions for light polarized along the E//c axis compared to the E//a axis, as the corresponding thermo-optic coefficient is higher for the E//c axis. Additionally, it should be noted that the Yb:YLF crystal is cooled from the upper side only, resulting in a downward shift of the center of optical path distortions in the vertical direction, making the distortion asymmetric. However, the lensing strength is similar in both horizontal and vertical directions, as the temperature rise is expected to be roughly equal in both directions. It is worth emphasizing that for the cryogenic Yb:YLF rod system, the estimated thermal lensing due to thermo-optic effect is much stronger compared to the population and bulging lens contributions.

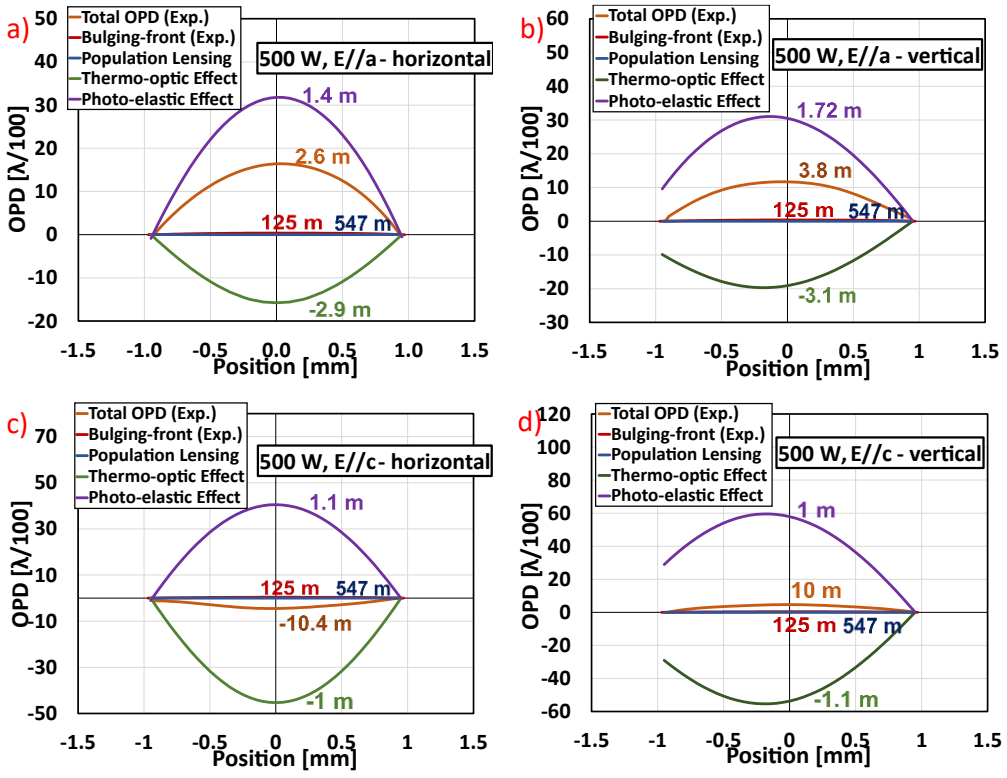

Fig. 9. Measured and estimated contributions to thermal lensing at cryogenic Yb:YLF (i) for E//a polarization in the (a) horizontal and (b) vertical directions; (ii) for E//c polarization in the (c) horizontal and (d) vertical directions at an absorbed pump power of 500 W.

We can now present Fig. 9, which shows a comparison of different sub-lensing contributions to thermal lensing for both E//a and E//c polarizations in horizontal and vertical directions at an

absorbed pump power of 500 W. The purpose is to determine the relative strengths of each sub-lensing effect with respect to each other. First, note that the front surface and back surface bulging contributions to total lensing, as shown in Fig. 7, is weak due to the use of undoped end cap sections. The contribution from population lensing is even smaller. These two contributions are found to be not polarization-dependent and are kept constant for all cases. However, they are considerably weak compared to other effects. The thermo-optic effect is a stronger contributor to lensing compared to bulging and population lensing. The effect is negative for both E//a and E//c axes in horizontal and vertical directions, with a higher strength of lensing in the E//c axis due to the higher thermo-optic coefficient of YLF. The last contribution to thermal lensing is the photo-elastic effect. Although some estimates of photo-elastic coefficients are available in the literature [25], their temperature dependence is not well known, so accurate calculation of the OPD induced by the photo-elastic effect is not possible. However, based on the photo-elastic coefficients from [25] and the strain tensor obtained from simulations, we estimate a strong positive thermal lensing due to the photo-elastic effect, which is consistent with our measurements. In our analysis, we have estimated the photo-elastic effect lens strength by subtracting all the other measured/calculated lensing strengths from the total measured thermal lens.

As we can see from Fig. 9 (a), for E//a polarized light, the lensing from bulging (~125 m) and population lensing (~547 m) are ignorable, and the calculated strength of thermo-optic effect lensing is around -2.9 m. We have measured a total lensing with a 2.6 m focal length for this case, which shows that the photo-elastic effect should be producing a very strong positive thermal lens with a focal length of 1.4 m. A similar argument shows that, the strength of photo-elastic effect thermal lens is around 1.7 m for E//a polarized light in the vertical direction (Fig. 9 (b)). Basically, for E//a polarized light, the thermal lens due to the photo-elastic effect is always stronger than the thermal lens due to thermo-optic effect, and hence we observe a relatively strong positive thermal lensing for this polarization (Fig. 5 (a)), in both horizontal and vertical directions.

For the E//c polarized light, the situation is very different and also more interesting. As an example, in the horizontal direction (Fig. 9 (c)), the overall measured thermal lens is -10.4 meters at 500 W absorbed pump power level. We see that, the contribution from bulging and population lensing is again ignorable. However, compared to E//a axis, the thermal lensing due to thermo-optic effect is stronger and generates a focal length of around -1 m. This is mostly because the thermo-optic coefficient for E//c polarization is 2-4 times larger compared to E//a polarization at cryogenic temperatures (see Table IX in [11]). Hence, for E//c polarization the thermal lens due to thermo-optic effect (-1 m) is as strong as thermal lens due to photo-elastic effect (1.1 m) for the horizontal direction, creating an overall thermal lens strength of -10.4 meters. A similar situation exist in the vertical direction: but this time the photo-elastic effect (1 m) is slightly stronger than the thermo-optic effect (-1.1 m), leading to a positive total thermal lensing of 10 m. Basically, for E//c polarized light, since the strength of photo-elastic and thermo-optic effect lensing are comparable, a weak overall thermal lens is measured, and the total thermal lens, which is the summation of negative thermal lensing from thermo-optic effect and positive thermal lensing from photo-elastic effect is small, and it can oscillate between positive and negative values (for the horizonal axis), as shown in Fig. 5 (b).

To look at the situation from another perspective, the estimated variation of thermo-optic and photo-elastic lens strengths as a function of absorbed pump power are shown in Fig. 10 (a-b) for the E//c axis in the horizontal direction. As we expected the distortions in the optical path become stronger when the absorbed power is increased in both lensing effects. Also, the absorbed power-dependent thermo-optic effect gives rise to negative lensing where the photo-elastic effect is always positive. Furthermore, we show the corresponding focal length strengths

as a function of absorbed power in Fig. 10 (c). Below 300 W absorption, the photo-elastic effect strength is slightly higher than the thermo-optic effect and that's why total thermal lensing is positive. When the absorbed power level is above 300 W, the thermo-optic effect becomes stronger and dominates the other effects, leading to negative total thermal lensing (the magnitude of dn/dT coefficient increases sharply with temperature). This occurs because the rate of increase of the thermo-optic effect is greater than the rate of increase of the photo-elastic effect, resulting in a stronger negative lensing effect as the absorbed power level increases.

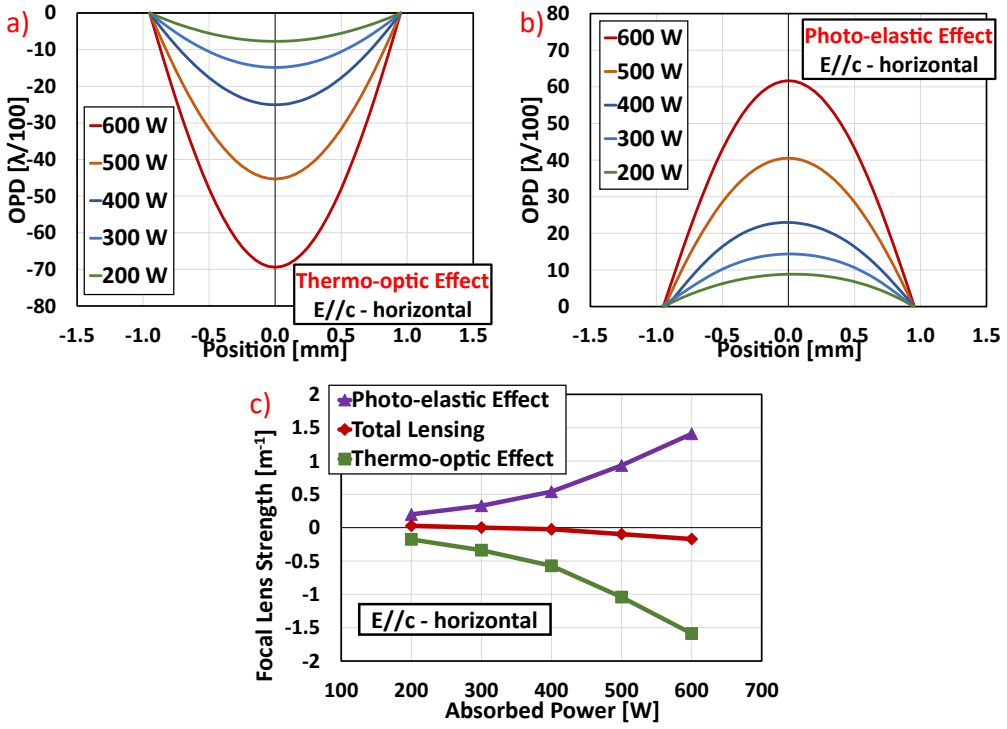

Fig. 10. Calculated variation of wavefront distortions (OPDs) due to (a) thermo-optic and (b) photo-elastic effects as a function of absorbed pump power level for E//c polarized light in the horizontal direction. (c) Calculated variation of thermal lensing focal length as a function of absorbed pump power level. The calculation shows the variation of photo-elastic thermal lens, thermo-optic thermal lens and overall thermal lens focal length.

4. Conclusion

In this work, we have provided a comprehensive investigation of the phenomenon of thermal lensing in cryogenic Yb:YLF systems. For the first time, we were able to measure population lensing in Yb:YLF and discovered that it is relatively weak, and we have estimated a very small polarizability difference parameter for Yb:YLF ($3\pm1.5 \times 10^{-34}$ m^3). Bulging lenses for both end faces were also measured and confirmed to be relatively weak due to the usage of undoped end caps in our crystals. Furthermore, we conducted calculations on the thermo-optic effect and found that it is much stronger than bulging and population lensing. This effect consistently leads to diverging/negative lensing and its strength is polarization dependent. In particular, the strength of the effect is greater when the electric field is parallel to the c-axis orientation, as compared E//a axis orientation. We also estimated the lensing contribution from the photo-elastic effect, and found that it is always converging/ positive, and its strength is also much larger than bulging and population lensing. Moreover, we have also studied the polarization and direction-dependence of total thermal lensing in Yb:YLF and found it to be quite

asymmetric, and much weaker for the E//c polarization, providing a great advantage to this polarization in high-power lasing experiments. Future work will focus on a deeper understanding of the contribution of the thermal lens from the photoelastic effect and the temperature dependence of the underlying photoelastic coefficients, thus facilitating the design and development of new generation Yb:YLF amplifiers.

5. Appendix

5.1 Formulas and Coefficients for Simulation of Yb:YLF Systems

In this study, a 960nm fiber-coupled diode system with up to 3 kW of CW output power is used as the pump source. Heat distribution depends on the parameters of the gain medium and the pump source parameters such as length-width-height of the crystal, cavity beam waist, pump beam quality factor (M^2), etc. Also, formulas should be arranged for rod-geometry in lab coordinates since we have a rod-type gain medium. The heat density distributions for rod geometries can be calculated using Eq. 4. [52,53]. Also, the parameters that are used to study heat load and thermal lens characteristics for the 1% Yb-doped YLF are given in Table 1.

$$Q(x,y,z) = C \exp\left[-\frac{2\left(x^2+y^2\right)^{\frac{N}{2}}}{w^N(z)} - \alpha z\right], \tag{4}$$

where $w(z)$ is the pump mode radius at position z (Eq. 6.), α is the absorption coefficient, N is the order of super gaussian beam, and C is a constant which can be calculated using:

$$C = \frac{P_{abs}\ FTL}{\int_0^L \int_{-D/2}^{D/2} \int_{-W/2}^{W/2} \exp\left[-\frac{2\left(x^2+y^2\right)^{\frac{N}{2}}}{w^N(z)} - \alpha z\right] dx dy dz}, \tag{5}$$

where P_{abs} is the absorbed pump power, FTL is the fractional thermal load, D is the depth, L is the length and W is the width of the gain medium.

$$w(z) = w_0 \sqrt{1 + \left(\frac{M^2 \lambda_p (z - z_0)}{n \pi w_0^2}\right)^2}, \tag{6}$$

where w_0 is the beam waist of the pump, M^2 is the beam quality factor of the pump, z_0 is the beam waist position and n is the refractive index of the gain medium at the pump wavelength.

Table 1. Corresponding parameters of the fiber-coupled pump and 1% Yb-doped YLF crystal for simulations. T in equations stands for temperature in Kelvin and .

Parameter	Abbreviation/ Symbol	Value/ Function
Absorbed Pump Power	P_{abs}	0 to 600 W
Pump Wavelength	λ_p	960 nm
Pump Beam Waist	w_0	1.05 mm
Pump Beam Quality Factor	M^2	220
Super Gaussian Order of Pump	N	20

Poisson's Ratio	v	0.33 [54]
Young's Modulus	E	7.6982×10^{10} Pa
Specific Heat Capacity	Cp	$300\ \mathrm{J/(kg.K)}$
Density	rho	$3950\ \mathrm{kg/m^3}$
Refractive Index of Extraordinary Axis	n_o	1.4485 [55]
Refractive Index of Ordinary Axis	n_e	1.4706 [55]
Fractional Thermal Load	FTL	1.7 x QD (Quantum Defect)
Effective Absorption Coefficient for 1% Yb doping (including pump saturation effect for 2.1 mm pump diameter**)**	α	$1\mathrm{x}10^{-14}P_{abs}^6 - 4\mathrm{x}10^{-11}P_{abs}^5 + 5\mathrm{x}10^{-8}P_{abs}^4 - 4\mathrm{x}10^{-5}P_{abs}^3 + 0.0148P_{abs}^2 - 2.9219P_{abs} + 311.8\ (\mathrm{m}^{-1})$
Length of the Doped Crystal	L_{doped}	20 mm
Length of the Undoped cups	$L_{unDoped}$	2x 3 mm
Depth of the Crystal	D	10 mm
Width of the Crystal	W	15 mm
Thermal Conductivity (E//a**)**	k_a	$14300T^{-1.41}\ \mathrm{W/(m.K)}$ [11]
Thermal Conductivity (E//c**)**	k_c	$21200T^{-1.42}\ \mathrm{W/(m.K)}$ [11]
Coefficient of Thermal Expansion (E//a**)**	α_{CTE_a}	$(-8 + 0.118T - 0.000146T^2)\mathrm{x}10^{-6}\ \frac{\mathrm{m}}{\mathrm{K}}$ [11,56]
Coefficient of Thermal Expansion (E//c**)**	α_{CTE_a}	$(-4.75 + 0.094T - 0.00015T^2)\mathrm{x}10^{-6}\ \frac{\mathrm{m}}{\mathrm{K}}$ [11,56]
Thermo-optic coefficient (E//a**)**	$\frac{dn_o}{dT}$	$(-0.10364 + 0.0010536T - 0.000053254T^2)\mathrm{x}10^{-6}\frac{1}{\mathrm{K}}$ [11]
Thermo-optic coefficient (E//c**)**	$\frac{dn_e}{dT}$	$(-0.038934 - 0.015482T - 0.000021742T^2)\mathrm{x}10^{-6}\frac{1}{\mathrm{K}}$ [11]

Funding

Deutsche Forschungsgemeinschaft (390715994); European Research Council (609920).

Acknowledgments

The authors acknowledge support from previous group members L. E. Zapata, K. Zapata for establishing the indium-bonding technology for YLF at CFEL-DESY.

Disclosures

The authors declare no conflicts of interest.

Data availability

Data underlying the results presented in this paper are not publicly available at this time but may be obtained from the authors upon reasonable request.

References

1. D. C. Brown, "The promise of cryogenic solid-state lasers," IEEE J. Sel. Top. Quantum Electron. **11**, 587–599 (2005).
2. D. J. Ripin, J. R. Ochoa, R. L. Aggarwal, and T. Y. Fan, "165-W cryogenically cooled Yb:YAG laser," **29**, 2154–2156 (2004).

3. J. G. Manni, J. D. Hybl, D. Rand, D. J. Ripin, J. R. Ochoa, T. Y. Fan, and S. Member, "100-W Q-switched Cryogenically," **46**, 95–98 (2010).
4. U. Demirbas, M. Kellert, J. Thesinga, S. Reuter, Y. Hua, M. Pergament, and F. X. Kärtner, "Recent progress in cryogenic Yb:YLF laser technology," **1201802**, 1 (2022).
5. D. J. Ripin, J. R. Ochoa, R. L. Aggarwal, T. Y. Fan, and S. Member, "300-W Cryogenically Cooled Yb:YAG Laser," **41**, 1274–1277 (2005).
6. L. E. Zapata, D. J. Ripin, and T. Y. Fan, "Power scaling of cryogenic Yb:LiYF_4 lasers," Opt. Lett. **35**, 1854 (2010).
7. D. E. Miller, J. R. Ochoa, and T. Y. Fan, "Cryogenically cooled, 149 W, Q-switched, Yb:$LiYF_4$ laser," Opt. Lett. **38**, 4260 (2013).
8. U. Demirbas, M. Kellert, J. Thesinga, Y. Hua, S. Reuter, M. Pergament, and F. X. Kärtner, "Highly efficient cryogenic Yb:YLF regenerative amplifier with 250 W average power," Opt. Lett. **46**, 3865 (2021).
9. M. Kellert, U. Demirbas, J. Thesinga, S. Reuter, M. Pergament, and F. X. Kärtner, "High power (>500W) cryogenically cooled Yb:YLF cw-oscillator operating at 995 nm and 1019 nm using E//c axis for lasing," Opt. Express **29**, 11674 (2021).
10. U. Demirbas, J. Thesinga, M. Kellert, F. X. Kärtner, and M. Pergament, "Detailed investigation of absorption, emission and gain in Yb:YLF in the 78–300 K range," Opt. Mater. Express **11**, 250 (2021).
11. R. L. Aggarwal, D. J. Ripin, J. R. Ochoa, and T. Y. Fan, " Measurement of thermo-optic properties of $Y_3Al_5O_{12}$, $Lu_3Al_5O_{12}$, $YAlO_3$, $LiYF_4$, $LiLuF_4$, BaY_2F_8, $KGd(WO_4)_2$, and $KY(WO_4)_2$ laser crystals in the 80-300 K temperature range," J. Appl. Phys. **98**, (2005).
12. U. Demirbas, H. Cankaya, Y. Hua, J. Thesinga, M. Pergament, and F. X. Kärtner, "20-mJ, sub-ps pulses at up to 70 W average power from a cryogenic Yb:YLF regenerative amplifier," Opt. Express **28**, 2466 (2020).
13. L. E. Zapata, M. Pergament, M. Schust, S. Reuter, J. Thesinga, C. Zapata, M. Kellert, U. Demirbas, A.-L. Calendron, Y. Liu, and F. X. Kärtner, "One-joule 500-Hz cryogenic Yb:YAG laser driver of composite thin-disk design," Opt. Lett. **47**, 6385 (2022).
14. Y. Liu, U. Demirbas, M. Kellert, J. Thesinga, H. Cankaya, Y. Hua, L. E. Zapata, M. Pergament, and F. X. Kärtner, "Eight-pass Yb:YLF cryogenic amplifier generating 305-mJ pulses," OSA Contin. **3**, 2722 (2020).
15. M. Pergament, M. Kellert, U. Demirbas, J. Thesinga, S. Reuter, Y. Hua, M. Kilinc, and F. X. Kärtner, "100mJ, 100W Cryogenically Cooled Yb:YLF Laser," 2022 Conf. Lasers Electro-Optics, CLEO 2022 - Proc. 2022–2023 (2022).
16. T. Y. Fan, D. J. Ripin, R. L. Aggarwal, J. R. Ochoa, B. Chann, M. Tilleman, and J. Spitzberg, "Cryogenic Yb^{3+}-doped solid-state lasers," IEEE J. Sel. Top. Quantum Electron. **13**, 448–458 (2007).
17. U. Demirbas, M. Kellert, J. Thesinga, S. Reuter, F. X. Kärtner, and M. Pergament, "Advantages of YLF host over YAG in power scaling at cryogenic temperatures: direct comparison of Yb-doped systems," Opt. Mater. Express **12**, 2508 (2022).
18. D. Strickland and G. Mourou, "Compression of amplified chirped optical pulses," Opt. Commun. **56**, 219–221 (1985).
19. P. A. Loiko, K. V. Yumashev, N. V. Kuleshov, and A. A. Pavlyuk, "Thermo-optic coefficients and thermal lensing in Nd-doped $KGd(WO_4)_2$ laser crystals," Appl. Opt. **49**, 6651–6659 (2010).
20. K. R. Hansen and J. Lægsgaard, "Thermal effects in high-power fiber amplifiers," Opt. InfoBase Conf. Pap. **19**, 1739–1741 (2011).
21. M. P. MacDonald, T. Graf, J. E. Balmer, and H. P. Weber, "Reducing thermal lensing in diode-pumped laser rods," Opt. Commun. **178**, 383–393 (2000).

22. M. Jalal AbdulRazzaq, A. K. Abass, and W. Yas Nassir, "Thermal Lensing Reduction in Conventional and Composite Nd:YAG Laser Rod," Eng. Technol. J. **34**, 2031–2035 (2016).
23. Y. T. Chang, Y. P. Huang, K. W. Su, and Y. F. Chen, "Comparison of thermal lensing effects between single-end and double-end diffusion-bonded Nd:YVO_4 crystals for $^4F_{3/2}\rightarrow{}^4I_{11/2}$ and $^4F_{3/2}\rightarrow{}^4I_{13/2}$ transitions," Opt. Express **16**, 21155 (2008).
24. K. V. Yumashev, A. N. Zakharova, and P. A. Loiko, "Photo-elastic effect, thermal lensing and depolarization in a-cut tetragonal laser crystals," Laser Phys. **26**, (2016).
25. V. V Zelenogorskii and E. A. Khazanov, "Influence of the photoelastic effect on the thermal lensin a YLF crystal," Quantum Electron. **40**, 40–44 (2010).
26. S. Chénais, F. Balembois, F. Druon, G. Lucas-Leclin, and P. Georges, "Thermal lensing in diode-pumped ytterbium lasers-Part I: Theoretical analysis and wavefront measurements," IEEE J. Quantum Electron. **40**, 1217–1234 (2004).
27. R. C. Powell, S. A. Payne, L. L. Chase, and G. D. Wilke, "Index-of-refraction change in optically pumped solid-state laser materials," Opt. Lett. **14**, 1204 (1989).
28. J. R. Silva, L. C. Malacarne, M. L. Baesso, S. M. Lima, L. H. C. Andrade, C. Jacinto, M. P. Hehlen, and N. G. C. Astrath, "Modeling the population lens effect in thermal lens spectrometry," Opt. Lett. **38**, 422 (2013).
29. N. Passilly, E. Haouas, V. Ménard, R. Moncorgé, and K. Aït-Ameur, "Population lensing effect in Cr:LiSAF probed by Z-scan technique," Opt. Commun. **260**, 703–707 (2006).
30. E. Anashkina and O. Antipov, "Electronic (population) lensing versus thermal lensing in Yb:YAG and Nd:YAG laser rods and disks," J. Opt. Soc. Am. B **27**, 363 (2010).
31. V. Hariton, C. P. Joao, H. Pires, M. Galletti, and G. Figueira, "Thermal lens analysis in a diode-pumped 10 Hz 100 mJ Yb:YAG amplifier," High Power Laser Sci. Eng. **8**, 1–8 (2020).
32. S. Chenais, F. Druon, and F. Balembois, "Thermal lensing measurements in diode-pumped Yb-doped GdCOB, YCOB, YSO, YAG and KGW," Opt. Mater. (Amst). **22**, 129–137 (2003).
33. I. B. Mukhin, O. V Palashov, E. A. Khazanov, A. G. Vyatkin, and E. A. Perevezentsev, "Laser and thermal characteristics of Yb:YAG crystals in the 80 — 300 K temperature range," Quantum Electron. **41**, 1045–1050 (2011).
34. J. L. Blows, P. Dekker, P. Wang, J. M. Dawes, and T. Omatsu, "Thermal lensing measurements and thermal conductivity of Yb:YAB," Appl. Phys. B Lasers Opt. **76**, 289–292 (2003).
35. P. Loiko, J. M. Serres, X. Mateos, H. Yu, H. Zhang, J. Liu, K. Yumashev, U. Griebner, V. Petrov, M. Aguilo, and F. Diaz, "Thermal Lensing and Multiwatt Microchip Laser Operation of Yb:YCOB Crystals," IEEE Photonics J. **8**, (2016).
36. J. E. Hellström, S. Bjurshagen, and V. Pasiskevicius, "Laser performance and thermal lensing in high-power diode-pumped Yb:KGW with athermal orientation," Appl. Phys. B Lasers Opt. **83**, 55–59 (2006).
37. P. A. Loiko, J. M. Serres, X. Mateos, K. V. Yumashev, N. V. Kuleshov, V. Petrov, U. Griebner, M. Aguiló, and F. Díaz, "Thermal lensing in Yb:$KLu(WO_4)_2$ crystals cut along the optical indicatrix axes," Laser Phys. Lett. **11**, (2014).
38. T. M. Klu, W. O. Crystals, P. A. Loiko, X. Mateos, N. V Kuleshov, A. A. Pavlyuk, K. V Yumashev, V. Petrov, U. Griebner, M. Aguiló, and F. Díaz, "Thermal-Lens-Driven Effects in N_g -Cut Yb-and Tm-Doped Monoclinic $KLu(WO_4)_2$ Crystals," **50**, 669–676 (2014).
39. P. Loiko, S. Manjooran, K. Yumashev, and A. Major, "Polarization anisotropy of thermal lens in Yb:$KY(WO_4)_2$ laser crystal under high-power diode pumping," Appl. Opt. **56**, 2937 (2017).

40. O. Kazasidis and U. Wittrock, "Simultaneous interferometric measurement of the temperature coefficient of the refractive index dn/dt and the coefficient of thermal expansion of laser crystals," Opt. InfoBase Conf. Pap. **22**, 3193–3196 (2014).
41. H. Vanherzeele, "Thermal lensing measurement and compensation in a continuous-wave mode-locked Nd:YLF laser," Opt. Lett. **13**, 369 (1988).
42. C.-W. Chen, Y.-H. Fang, C.-Y. Cho, and H.-C. Liang, "Investigation of anisotropic thermal lens effect in a dual-polarized Nd:YLF laser," Opt. Lett. **46**, 94 (2021).
43. P. J. Hardman, W. A. Clarkson, G. J. Friel, M. Pollnau, and D. C. Hanna, "Energy-transfer upconversion and thermal lensing in high-power end-pumped Nd: YLF laser crystals," IEEE J. Quantum Electron. **35**, 647–655 (1999).
44. J. E. Murray, "Pulsed Gain and Thermal Lensing of Nd:$LiYF_4$," IEEE J. Quantum Electron. **19**, 488–491 (1983).
45. A. Jolly, S. Vidal, and J. Boullet, "Thermal lensing effects in rod-based Tm^{3+}:YLF amplifiers versus pump and cooling conditions," Laser Phys. **28**, (2018).
46. O. N. Ereme, N. A. Egorov, N. G. Zakharov, A. P. Savikin, and V. V Sharkov, "Investigating a thermal lens in a Tm : YLF crystal under intense diode pumping," America (NY). 676–679 (2009).
47. X. Zhang, Y. Wang, L. Li, and Y. Ju, "Heat generation and thermal lensing in end-pumped Tm,Ho : YLF laser crystals," J. Phys. D. Appl. Phys. **40**, 6930–6935 (2007).
48. U. Demirbas, J. Thesinga, M. Kellert, M. Pergament, and F. X. Kärtner, "Temperature and doping dependence of fluorescence lifetime in Yb:YLF (role of impurities)," Opt. Mater. (Amst). **112**, (2021).
49. I. Tamer, S. Keppler, M. Hornung, J. Körner, J. Hein, and M. C. Kaluza, "Spatio-Temporal Characterization of Pump-Induced Wavefront Aberrations in Yb^{3+}-Doped Materials," Laser Photonics Rev. **12**, 1–9 (2018).
50. S. Püschel, S. Kalusniak, C. Kränkel, and H. Tanaka, "Temperature-dependent radiative lifetime of Yb:YLF: refined cross sections and potential for laser cooling," Opt. Express **29**, 11106 (2021).
51. O. L. Antipov, D. V. Bredikhin, O. N. Eremeykin, A. P. Savikin, E. V. Ivakin, and A. V. Sukhadolau, "Electronic mechanism for refractive-index changes in intensively pumped Yb:YAG laser crystals," Opt. Lett. **31**, 763 (2006).
52. T. Taira, J. Saikawa, T. Kobayashi, and R. L. Byer, "Diode-pumped tunable Yb: YAG miniature lasers at room temperature: Modeling and experiment," IEEE J. Sel. Top. Quantum Electron. **3**, 100–104 (1997).
53. Z. Ma, D. Li, J. Gao, N. Wu, and K. Du, "Thermal effects of the diode end-pumped Nd:YVO_4 slab," Opt. Commun. **275**, 179–185 (2007).
54. D. C. Brown, S. Tornegård, J. Kolis, C. McMillen, C. Moore, L. Sanjeewa, and C. Hancock, "The application of cryogenic laser physics to the development of high average power ultra-short pulse lasers," Appl. Sci. **6**, 1–74 (2016).
55. T. Radhakrishnan, "Temperature variation of the refractive index of lithium fluoride," Proc. Indian Acad. Sci. - Sect. A **31**, 224–228 (1950).
56. R. J. Corruccini and J. J. Gniewek, "Thermal expansion of technical solids at low temperatures; a compilation from the literature," NBS Monogr. 28 (1961).